

Punjab University  
Journal of Mathematics (ISSN 1016-2526)  
Vol. 51(4)(2019) pp. 113-129

## Active Contour Model Based on Local Signed Pressure Force Functions

Shafaq-zu-Fishan<sup>1</sup>, Lutful Mabood<sup>2</sup>, Haider Ali<sup>3</sup>, Noor Badshah<sup>4</sup>

<sup>1,2,3</sup> Department of Mathematics, University of Peshawar, Pakistan.

<sup>4</sup> Department of Basic Sciences, University of Engineering and Technology, Peshawar, Pakistan.  
<sup>1,2,3,4</sup> Email: shafaqshakir92@gmail.com, lathizm@gmail.com, haider\_uop99@yahoo.com,  
noor2knoor@gmail.com

Received: 20 March, 2018 / Accepted: 09 July, 2018 / Published online: 04 March, 2019

**Abstract.** In image segmentation, intensity inhomogeneity is one of the main problems in case of region-based level set methods. Another problem is to segmenting images having average intensity background and multi-intensity objects in foreground. Therefore, in this paper we present a new model for segmentation of such kind of images by utilizing generalized averages in our proposed local sign pressure force function which is further incorporated into the Geodesic active contour model to obtain the evolution equation. Moreover, for the segmentation of average intensity background images we used a difference image in our local sign pressure force function and also calculated the bounds for the parameters  $\alpha$  and  $\beta$ . Experimental section validate that the results of our proposed functional is better than existing traditional models.

**AMS (MOS) Subject Classification Codes:** 35S29; 40S70; 25U09

**Key Words:** Image segmentation, SBGFLS model, Level set method, and Signed pressure force function.

### 1. INTRODUCTION

The process in which we divide an image into various segments such that, each segment is homogeneous is called image segmentation and its play a crucial role in many fields like image processing, computer vision etc. The primary role of image segmentation is to distinguish foreground from background [3, 4, 8, 9, 12]. The variational techniques used for segmentation of images can be categorized into two categories; one is known as edge based models and the other one is called region based models. In edge based models an edge detector function is design in such a way that it stops the motion of contour at the boundaries of the objects [3, 5, 6, 9]. In such kind of edge detector functions the gradient of a image play a crucial role due to which it utilizes only local information of a given image therefore these models are not able to segment noisy images. In contrast, region based segmentation models are usually found to use image global information based on

statistical terms such as mean, standard deviation, etc, to find out objects boundaries [4, 10, 15, 16]. Both of these methods have some pros and cons in various types of images like inhomogeneous and noisy images. There are also other models which utilize both the edge, region or local information [11, 17] to segment images named as hybrid models to handle inhomogeneity in images. But still the problem of inhomogeneity which usually occur in medical images like; MRI and CT images are not solely solved and many models have been develop [10, 17] to tackle it. Secondly the segmentation of images having average intensity background and multi-intensities objects in the foreground create problem and many latest models [1, 18] are not working well in these kinds of images. The reason behind this is the fact that most models use original image in which it is difficult to segment objects with different intensities, because most of the models work on assumption that the objects must be of same intensities. So to overcome this deficiency we will use a difference image instead of original image in our proposed function. Actually the difference image is a clean version of the given image in which the foreground become of the same intensity which make the segmentation task easier. Furthermore, for segmenting images having intensity inhomogeneity we used generalized mean in our proposed function and by experimental results we showed that its results are much accurate as compared to other traditional models.

The rest of the paper is organized as follows. Section 2 present review of previous work, section 3 shows our proposed model, section 4 present experimental results, while section 5 contain some conclusive remarks.

## 2. PREVIOUS WORKS

**2.1. Geodesic Active Contours (GAC) Model.** Let  $w_0 : \Omega \rightarrow \mathbb{R}$  is an observed image defined on a bounded open subset  $\Omega$  of  $\mathbb{R}^2$ , and  $C(w_0) : [0, 1] \rightarrow \mathbb{R}^2$  be a parameterized plane curve in  $\Omega$ . Then the GAC model [3] proposed the following minimization problem:

$$F_{GAC}(C) = \int_0^1 |C'(w_0)| g(|\nabla w_0(C(w_0))|) dv, \quad (2.1)$$

where the edge detector function is denoted by  $g$ , and is defined for  $p \geq 1$  and a Gaussian  $G_\sigma(x, y)$  as follow:

$$g(|\nabla w_0|) = \frac{1}{1 + |\nabla G_\sigma(x, y) * w_0|^p}.$$

Actually, GAC model is a modified form of snake model [9] which aim is to overcome the limitation of snake model such as; inflexibility of the active contours for topological changes and dependence of the segmentation results strictly on the choice of different parametrization of the active contours. Further, it can be written as;

$$\int_0^1 |C'(w_0)| dv = \int_0^{L(C)} ds,$$

where  $ds$  represent the length of Euclidean element and  $L(C)$  is the Euclidean length of the curve  $C$  [3, 4], hence equation (2. 1) becomes:

$$\min_C F_{GAC}(C) = \int_0^{L(C)} g(|\nabla w_0(C(w_0))|) ds. \quad (2.2)$$

Next, the direction for which the functional in equation (2. 2) decreases most rapidly provides us the following minimization flow:

$$\frac{\partial C}{\partial t} = g\kappa \vec{N} - (\nabla \cdot g \vec{N}) \vec{N}, \quad (2. 3)$$

here  $\kappa$  represent the Euclidean curvature, and the unit normal vector to the curve is denoted by  $\vec{N}$ . For derivation details interested readers are refer to [3]. Now in level set formulation [13], the evolution equation can be written as:

$$\frac{\partial \phi}{\partial t} = g(|\nabla w_0|) \left( \operatorname{div}\left(\frac{\nabla \phi}{|\nabla \phi|}\right) + \alpha \right) |\nabla \phi| + \nabla g \cdot \nabla \phi, \quad (2. 4)$$

where  $\alpha |\nabla \phi|$  is used to control the moment of contour from over expanding or from over shrinking and is known as balloon force with parameter  $\alpha$ . And  $\phi$  is the level set function. Since the classical snakes and active contour models mostly depend on image gradient information so it only capture those objects whose boundaries are defined by gradient. Therefore, these models are not able to preform well in noisy images one may use Gaussian isotropic smoothing but it also smooth the edges as well and thus the segmentation task become more hinder. Hence to handle this problem Chan-Vese (CV) model [4] was introduced which rely on image global information instead of image gradient.

**2.2. Chan-Vese model (CV).** A commonly used model for segmentation of images is the active contour model without edges proposed by Chan and Vese (CV) [4]. CV model is the special case of Mumford-Shah (MS) model [12], when restricted to only two phases therefore CV model is also known as piecewise constant Mumford-Shah model. Let  $\Gamma$  is the unknown boundary of the objects in the given image  $w_0$  defined on domain  $\Omega$ , then the CV model proposed the following minimization problem:

$$\begin{aligned} E_{CV} &= \lambda_1 \int_{\text{inside}(\Gamma)} |w_0(x, y) - c_1|^2 dx \\ &+ \lambda_2 \int_{\text{outside}(\Gamma)} |w_0(x, y) - c_2|^2 dx, \quad (x, y) \in \Omega, \end{aligned} \quad (2. 5)$$

here  $c_1$  and  $c_2$  are two constants and represent the value of average intensities of the pixels inside and outside of  $\Gamma$  respectively. Now utilizing the technique of level set formulation [2, 14] we can assume:

$$\begin{cases} \Gamma = \{(x, y) \in \Omega : \phi(x, y) = 0\}, \\ \text{inside}(\Gamma) = \{(x, y) \in \Omega : \phi(x, y) > 0\}, \\ \text{outside}(\Gamma) = \{(x, y) \in \Omega : \phi(x, y) < 0\}. \end{cases} \quad (2. 6)$$

The values of  $c_1$  and  $c_2$  can be obtained by minimizing equation (2. 5), with respect to two constants  $c_1$  and  $c_2$  as follow:

$$c_1 = \frac{\int_{\Omega} w_0 H(\phi) dx dy}{\int_{\Omega} H(\phi) dx dy}, \quad c_2 = \frac{\int_{\Omega} w_0 (1 - H(\phi)) dx dy}{\int_{\Omega} (1 - H(\phi)) dx dy}. \quad (2. 7)$$

By adding the area and length energy terms into equation (2. 5), and minimization of them leads us to the following evolution equation:

$$\frac{\partial \phi}{\partial t} = \delta(\phi) \left[ \mu \nabla \cdot \left( \frac{\nabla \phi}{|\nabla \phi|} \right) - v - \lambda_1 (w_0 - c_1)^2 + \lambda_2 (w_0 - c_2)^2 \right], \quad (2. 8)$$

where  $v \geq 0, \mu \geq 0, \lambda_1 > 0, \lambda_2 > 0$  are fixed parameters and to be tuned according to the given images.  $v$ , control the propagation speed of the curve,  $\mu$  control the smoothness of the curve while  $\lambda_1, \lambda_2$  are fixed parameters. In addition,  $H(\phi)$  is the Heaviside function and  $\delta(\phi)$  is the derivative of the Heaviside function known as dirac delta function. Usually, the regularized form of Heaviside and delta functions are used as given:

$$H_\epsilon(x) = \frac{1}{2}\left(1 + \frac{2}{\pi} \arctan\left(\frac{x}{\epsilon}\right)\right), \quad \delta_\epsilon(x) = \frac{\epsilon}{\pi(\epsilon^2 + x^2)} \quad x \in \mathbb{R}. \quad (2.9)$$

The performance of CV model are much accurate in two phases image segmentation in which background and foreground consist on constant intensities. However, CV model does not work properly in those images which are suffered from intensity inhomogeneity. Therefore, to overcome the limitation of the CV model many new algorithms were developed such as [10, 11, 17] etc.,

**2.3. The SBGFRLS Model (CVB).** The CVB model [18] is another attempt in variational modeling which gives better results than GAC and CV models. Based on the concept of Spf function in [16], the CVB model defined the Spf function as follow:

$$E_{Spf}(w_0(x, y)) = \frac{w_0(x, y) - \frac{c_1 + c_2}{2}}{\max\left|w_0(x, y) - \frac{c_1 + c_2}{2}\right|}, \quad (x, y) \in \Omega, \quad (2.10)$$

here again  $c_1$  and  $c_2$  are the averages as already defined in equation (2. 7). The Spf function has same properties as that of the edge detector function as it also takes values in the interval of  $[-1, 1]$ , and its signs modulates inside and outside of the object, and hence the contour shrinks and expands from outside and inside of the object respectively. Next, based on the edge detection property of the Spf function, it is substituted in equation (2. 4) to obtain the following equation:

$$\frac{\partial \phi}{\partial t} = E_{Spf}(w_0(x, y)) \left( \operatorname{div}\left(\frac{\nabla \phi}{|\nabla \phi|}\right) + \alpha \right) |\nabla \phi| + \nabla E_{Spf}(w_0(x, y)) \cdot \nabla \phi. \quad (2.11)$$

Furthermore, equation (2. 11) can be expresses as in the form of the following evolution equation [18]:

$$\frac{\partial \phi}{\partial t} = E_{Spf}(w_0(x, y)) \cdot \alpha |\nabla \phi|, \quad (x, y) \in \Omega. \quad (2.12)$$

Usually, the curvature term  $\nabla \cdot \left(\frac{\nabla \phi}{|\nabla \phi|}\right)$  is used in the traditional level set methods for the regularization of the level set function  $\phi$ . On the other hand in CVB model the Gaussian kernel filtering is used instead of the curvature term as the initial condition of the function. Therefore, for the regularization of the level set function Gaussian filtering process is utilized and the regularization strength is control by the standard deviation of the Gaussian filter, just as the parameter  $\mu$  does in equation (2. 8) [18, 19]. Finally, the simple finite difference scheme is implemented to obtain the solution. This model works in those images having piecewise constant regions. But since the averages used in this model are that of CV model, so it has the same limitation as that of the CV model, such as the inefficiency in handling images suffered from severe intensity inhomogeneity [18]. It is important to note that the Spf function in equation (2. 10) and the curve evolution equation (2. 12)

) are based on the assumption that an image has only one object of homogeneous intensity. Thus, it is clear that the CVB model can not work well when there are multi-objects in the image having different intensities [19]. It may work in some multi-objects images having the background intensity either the maximum or the minimum, however, similar to the CV model, this model is unable to handle images having background with average intensity [18, 19]. Furthermore, in case of multi-objects images having either maximum or minimum intensity background the CVB model works only for particular images [18, 19].

**2.4. Multi-Region Segmentation (MRS) Model.** In [1] Ali et al. proposed generalized averages and a new sign pressure force function for a given image. Let  $w_0$  be an observed image then the generalized averages inside and outside of an active contour are defined as follow:

$$G_{c_1} = \frac{\int_{\Omega} w_0^{\beta} H(\phi) dx dy}{\int_{\Omega} w_0^{\beta-1} H(\phi) dx dy}, \quad (2.13)$$

$$G_{c_2} = \frac{\int_{\Omega} w_0^{\beta} (1 - H(\phi)) dx dy}{\int_{\Omega} w_0^{\beta-1} (1 - H(\phi)) dx dy}, \quad (2.14)$$

where  $\beta$  is any real number. The above family of averages is named as *Avg – family*. Where the new Spf function known as generalized sign pressure force function (GSpf) is defined as:

$$E_{GSpf} = \frac{w_0(x, y) - \frac{G_{c_1} + G_{c_2}}{2}}{\max\left(\left|w_0(x, y) - \frac{G_{c_1} + G_{c_2}}{2}\right|\right)}, \quad (2.15)$$

where  $(x, y) \in \Omega$ . Hence by replacing  $E_{Spf}(w_0(x, y))$  in equation (2. 12) by GS pf function which is defined in equation (2. 15) gives the following evolution equation:

$$\frac{\partial \phi}{\partial t} = \alpha E_{GSpf} |\nabla \phi| \text{ in } \Omega, \quad (2.16)$$

$$\phi(t, x, y) = \phi_0(x, y), \text{ in } \Omega. \quad (2.17)$$

Since the PDE (2. 16) contains the generalized statistical image intensity information due to which the contour moves to the edges which truly represent the edges of the objects. But this model does not work well in images having severe intensity inhomogeneity as shown in experimental section.

### 3. PROPOSED MODEL (LSpf)

This section contain our proposed model LSpf based on the concept of generalized averages [7] and a new local signed pressure force function (LSpf). As the MRS model is unable to work in images having intensity inhomogeneity. So to overcome this deficiency we propose our new model utilizing generalized mean and incorporating local image information in the Spf function. First of all we define generalized mean and some basic results as follow.

**Definition 1.** Let  $p$  is the exponent of the positive real numbers  $x_1, \dots, x_k$ , such that  $p$  is non-zero real number then the generalized mean or power mean [7] is defined as:

$$M_p(x_1, x_2, \dots, x_k) = \left( \frac{1}{k} \sum_{i=1}^k x_i^p \right)^{\frac{1}{p}}. \quad (3. 18)$$

**Lemma 1.** In particular, for  $p = 0$  equation (3. 18) reduced to the geometric mean given by:

$$M_0(x_1, x_2, \dots, x_k) = \sqrt[k]{\prod_{i=1}^k x_i}.$$

**Lemma 2.** When  $p \rightarrow -\infty$  and  $p \rightarrow +\infty$  then equation (3. 18) represents the minimum and maximum respectively as follows:

$$M_{-\infty}(x_1, x_2, \dots, x_k) = \lim_{p \rightarrow -\infty} M_p(x_1, x_2, \dots, x_k) = \min\{x_1, x_2, \dots, x_k\},$$

$$M_{+\infty}(x_1, x_2, \dots, x_k) = \lim_{p \rightarrow \infty} M_p(x_1, x_2, \dots, x_k) = \max\{x_1, x_2, \dots, x_k\},$$

**Lemma 3.** When  $p = -1, 1$  and  $2$  then equation (3. 18) represents the geometric mean, arithmetic mean and quadratic mean respectively as follows:

$$M_{-1}(x_1, x_2, \dots, x_k) = \frac{k}{\frac{1}{x_1} + \frac{1}{x_2} + \dots + \frac{1}{x_k}}.$$

For  $p = 1$ ,

$$M_1(x_1, x_2, \dots, x_k) = \frac{x_1 + x_2 + \dots + x_k}{k}.$$

For  $p = 2$ ,

$$M_2(x_1, x_2, \dots, x_k) = \sqrt{\frac{x_1^2 + x_2^2 + \dots + x_k^2}{k}}.$$

The advantage of the generalized averages over the traditional mean is that by a single parameter  $p$  we can just get different types of averages according to different type of images, due to which our proposed model is able to tackle the intensity inhomogeneity as well as those images having average intensity background as shown in figure 5. Furthermore, we designed our proposed LSpf as follows:

$$E_{LSpf}(w_0(x, y)) = \frac{(w_0(x, y) - v(x, y)) - \frac{d_1 + d_2}{2}}{\max\left(\left|(w_0(x, y) - v(x, y)) - \frac{d_1 + d_2}{2}\right|\right)}, \quad y \in \Omega, \quad (3. 19)$$

where  $v(x, y) = g_k * w_0(x, y) - w_0(x, y)$  is the difference image and  $g_k$  is a averaging convolution operator with  $k \times k$  window size,  $d_1$  and  $d_2$  are the average intensities of the difference image inside and outside of the active contour, respectively. The main theme behind the uses of difference image is that it utilized the local information of the image and local regions of a image are more likely to have homogeneous. Therefore, our proposed

LSpf can handle intensity inhomogeneity very well. Moreover, we use the generalized mean as define in equation (3. 18) to calculate the values of  $d_1$  and  $d_2$  as follows:

$$d_1(\phi) = \left( \frac{\int_{\Omega} v^p H(\phi) dx dy}{\int_{\Omega} H(\phi) dx dy} \right)^{\frac{1}{p}}, \quad d_2(\phi) = \left( \frac{\int_{\Omega} v^p (1 - H(\phi)) dx dy}{\int_{\Omega} (1 - H(\phi)) dx dy} \right)^{\frac{1}{p}}, \quad (3.20)$$

where  $p$  is any non-zero real number. Next, we incorporate LSpf in equation (2. 4) to obtain the following evolution equation:

$$\frac{\partial \phi}{\partial t} = E_{LSpf}(w_0(x, y)) \left( \operatorname{div} \left( \frac{\nabla \phi}{|\nabla \phi|} \right) + \alpha \right) |\nabla \phi| + \nabla E_{LSpf}(w_0(x, y)) \cdot \nabla \phi. \quad (3.21)$$

For further implementation and numerical solution of the above equation interested readers are refired to [16].

**3.1. Image Segmentation for Average Intensity Background.** Since we have already discussed in section (2.3) that the CV and CVB model cannot perform well in those images having average intensity background and having maximum or minimum intensity objects in the foreground [18]. So to overcome this deficiency of segmenting images in case of average intensity background, we adopted a new technique by utilizing a product image which is based on our observation and experiments as follows. Let we have an image  $I$  and denote its average, maximum and minimum intensities by  $I_{avg}$ ,  $I_{max}$  and  $I_{min}$  respectively, as follows then:

$$I_{min} < I_{avg} < I_{max} \quad (3.22)$$

Now we consider two images  $I_1$  and  $I_2$  which are obtained by subtracting a constant values from the original image  $I$ , i.e.  $I_1$  and  $I_2$  be in the form  $I - \alpha$  and  $I - \beta$  respectively, where  $\alpha$  and  $\beta$  are two constant values, and considering the product of these two images denoted by,  $I_{pdt}$ , i.e.  $I_{pdt} = I_1 * I_2$ . Now  $\alpha$  and  $\beta$  are chosen such that,  $I_{max} - \alpha > 0$ ,  $I_{max} - \beta > 0$ ,  $I_{min} - \alpha < 0$ ,  $I_{min} - \beta < 0$ ,  $I_{avg} - \alpha > 0$  and  $I_{avg} - \beta < 0$ .

$$\frac{I_{max} + I_{min}}{2} < \alpha < \frac{I_{max} + I_{avg}}{2} \quad (3.23)$$

and

$$\frac{I_{avg} + I_{min}}{2} < \beta < \frac{I_{max} + I_{min}}{2} \quad (3.24)$$

Now we just replace the original image  $w_0(x, y)$  by the product image  $I_{pdt}$  in the difference image  $v(x, y)$ , i.e. its become  $v(x, y) = g_k * I_{pdt} - I_{pdt}$ .

#### 4. EXPERIMENTAL RESULTS

This section demonstrates the experimental results of our proposed model LSpf on medical inhomogeneous and on average intensity background images. The LSpf model was implemented by Matlab 7.9 on a core i3 personal computer with 2.40GHz processor, 2GB RAM and window 7 operating system. The first four experiments represents the performance of our proposed model in inhomogeneity of medical images, while other experiments indicate the results of proposed model in average intensity background. In each figure first row and second row show the results of CVB and MRS , while third row shows the results of LSpf. Also in each experiment the initial contour keep same for both the models except for experiments 2 and 4 in which the initial contour keep small for CVB

model as compared to LSpf for obtaining nice results. Figures 1, 2, 3, and 4 are MR brain, chest, and veins images respectively with intensity inhomogeneity, figures 1(c), 2(c), 3(c), and 4(c) represent the uncomplete task of CVB in inhomogeneity while figures 1(f), 2(f), 3(f), and 4(f) represents the poor performance of MRS. In contrast figures 1(i), 2(i), 3(i), and 4(i) show the complete segmented results of LSpf in inhomogeneity in medical MR images. Next experiments illustrate the results of LSpf in average intensity background images. In all these experiments the values of  $\mu$  and generalized mean( $p$ ) keep constant which are 20 and 2 respectively, except experiment 6 in which the value of  $p$  is 4. Figure 5 is an average intensity background image having two objects with maximum and minimum intensities, in which CVB and MRS fail to detect both objects while LSpf segment it very well as compared to CVB and MRS as shown in figure 5(i). Figures 6 and 7 are tough images having average intensity background and multi-intensities objects in it. CVB model and MRS model are able to detect only three objects in experiment 6 as seen from figures 6(c) and 6(f) respectively, while LSpf detect five objects in the same image as shown in figure 6(i). The result of CVB model carry no meaning in figure 7, i.e. it is not able to segment even a single object in it, while the segmented result of LSpf is pretty good. Although, in the last two experiments the performance of LSpf is not seem successful, but it is far better than traditional models.

Furthermore for quantitative comparison we used the Jaccard similarity (JS) for different models. For this we consider the segmented region by R1 and the ground truth (GT) by R2 , then the JS is the ratio of the areas of the intersection by the union of the regions, i.e.  $JS(R_1, R_2) = \frac{|R_1 \cap R_2|}{|R_1 \cup R_2|}$ . For better results we want JS to be close to 1. The GT used in this paper is obtained manually in the following way: based on the maximum intensity we set a threshold value and then we choose GT as image  $\leq$  threshold value. Now based on our observations we have found out the mean and standard deviation of JS values for different types of images as follow: For images having minimum intensity background the JS values of CVB model is  $0.79 \pm 0.2$ , MRS model is  $0.8 \pm 0.04$  and for proposed model is  $0.93 \pm 0.03$ . While for images having average intensity background the JS values of CVB model is  $0.6 \pm 0.3$ , MRS model is  $0.7 \pm 0.2$  and for proposed model is  $0.9 \pm 0.3$ . Finally, to show the effects of the parameters  $\alpha$  and  $\beta$  we used a synthetic image of multi-intensity objects having average intensity background as shown in figure 8. Now it can be observed from figure 8 that for different choices of  $\alpha$  and  $\beta$  we get different and poor segmentation results as shown in figures 8(b) and 8(c). But on the other hand if we choose proper values for  $\alpha$  and  $\beta$  as given in equations (3. 23) and (3. 24) we will get an accurate segmentation result as shown in figure 8(d).

## 5. CONCLUSION

In this paper, we developed two techniques for segmenting two types of images i.e. those images having inhomogeneity and images having average intensity background using generalized mean and a difference/product of image in our proposed LSpf function respectively. We tested our proposed techniques on some real MR images having intensities inhomogeneity and some synthetic images having average intensity background with maximum, minimum, and multi-intensities objects in the foreground. The experimental results

describes that our proposed model are more accurate in segmenting images as compared to CVB and the latest MRS models and more robust in numbers of iterations.

## 6. ACKNOWLEDGMENTS

We greatly acknowledge all reviewers for their constructive criticism, invaluable comments that greatly enhance this article. I am also thankful to Mr. Zia Ul Mabood, student at Bradford University, for proofreading.

## 7. CONFLICT OF INTEREST

All the authors in this paper contributed equally and have no conflict of interest to disclose.

## REFERENCES

- [1] H. Ali, N. Badshah, K. Chen, G. A. Khan and N. Zikria, *Multiphase segmentation based on new signed pressure force functions and one level set function*, Turkish Journal of Electrical Engineering & Computer Sciences **1**, (2017) 1–30.
- [2] M. Alyamac and K. F. Almaz, *Assesment of Samarandache Curves in The Null Cone  $Q^2$* , Punjab Univ. j. math. **51**, No. 3 (2019) 101–112.
- [3] V. Caselles, R. Kimmel and G. Sapiro, *Geodesic active contours*, International Jornal of Computer Vision **22**, No. 1 (1997) 61–79.
- [4] T. F. Chan and L. A. Vese, *Active contours without edges*, IEEE Transactions on Image Processing **10**, No. 2 (2001) 266–277.
- [5] C. Gout, C. L. Guyader and L. A. Vese, *Segmentation under geometrical conditions with geodesic active contour and interpolation using level set method*, Numerical Algorithms **39**, (2005) 155–173.
- [6] C. L. Guyader and C. Gout, *Geodesic active contour under geometrical conditions theory and 3D applications*, Numerical Algorithms **48**, (2008) 105–133.
- [7] O. Holder, *Die Mathematische Methode*, Trade paperback (US), Springer, 1924.
- [8] M. Jeon, M. Alexander, W. Pedrycz and N. Pizzi, *Unsupervised hierarchical image segmentation with level set and additive operator splitting*, Physical Review Letters **26**, No. 10 (2005) 1461–1469.
- [9] M. Kass, A. Witkin and D. Terzopoulos, *Active contours models*, International Jornal of Computer Vision (1988) 321–331.
- [10] C. M. Li, C. Kao, J. Gore and Z. Ding, *Implicit active contours driven by local binary fitting energy*, IEEE Conference on Computer Vision and Pattern Recognition, 2007.
- [11] L. Mabood, H. Ali, N. Badshah, K. Chen and G. A. Khan, *Active contours textural and inhomogeneous object extraction*, Pattern Recognition **55**, (2016) 87–99.
- [12] D. Mumford and J. Shah, *Optimal approximation by piecewise smooth functions and associated variational problems*, Communications on Pure Applied Mathematics **42**, (1989) 577–685.
- [13] S. Osher and J. A. Sethian, *Fronts propagating with curvature-dependent speed: algorithms based on Hamilton-Jacobi formulations*, J. Comput. Phys. **79**, No. 1 (1988) 12–49.
- [14] S. Osher and R. Fedkiw, *Level Set Methods and Dynamic Implicit Surfaces*, Springer: New York, NY, 2003.
- [15] L. A. Vese and T. F. Chan, *A multiphase level set framework for image segmentation using the Mumford and Shah model*, Int. J. Computer Vision **50**, No. 3 (2002) 271–293.
- [16] C. Y. Xu, A. Yezzi and J. L. Prince, *On the relationship between parametric and geometric active contours*, Processing of 34th Asilomar Conference on Signals Systems and Computers (2000) 483–489.
- [17] X. F. Wang, D. S. Huang and H. Xu, *An efficient local Chan-Vese model for image segmentation*, Pattern Recognition **43**, (2010) 603–618.
- [18] K. Zhang, L. Zhang, H. Song and W. Zhou, *Active contours with selective local or global segmentation: A new formulation and level set method*, Image and Vision Computing **28**, (2010) 668–676.
- [19] C. Zhang, Y. Zhang and Z. Lin, *Automatic face segmentation based on the level set method*, National Conference on Information Technology and Computer Science (2012) 678–681.

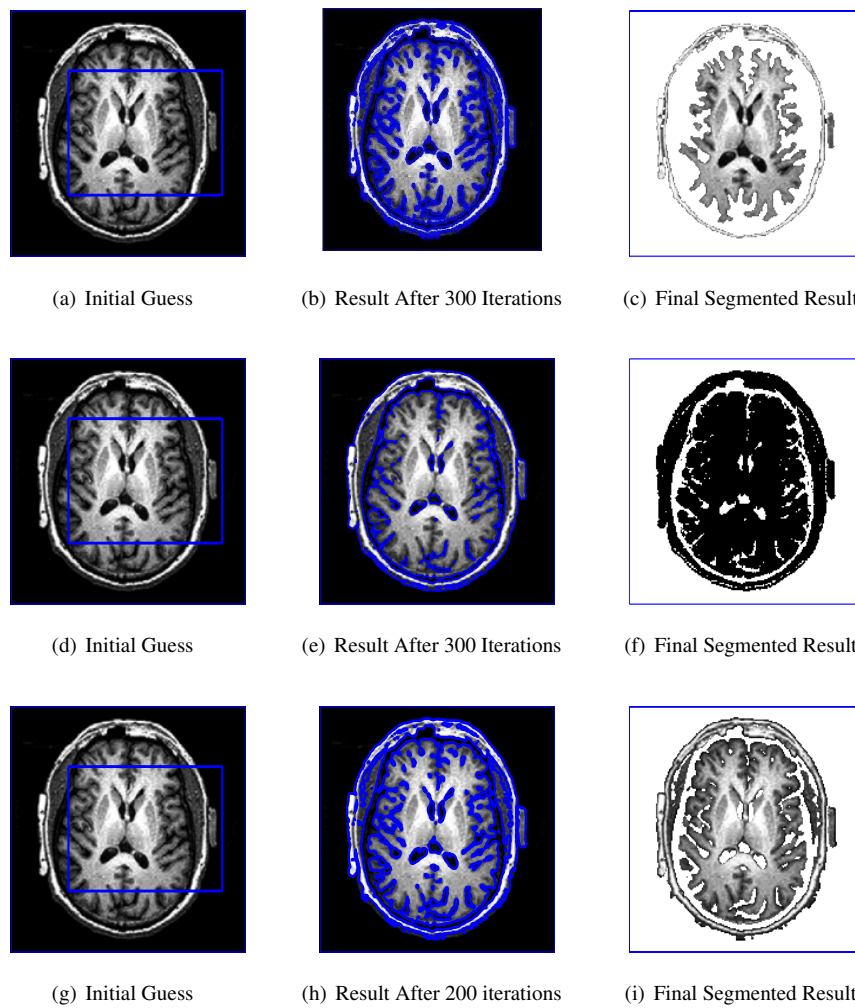


FIGURE 1. A real MR image of brain having inhomogeneity. Figure(c) and figure(f) shows the incomplete result of the CVB model and MRS model respectively, while figure(i) is the result of our proposed model; The parameters used for LSpf are  $p = 2$  and  $\mu = 10$ .

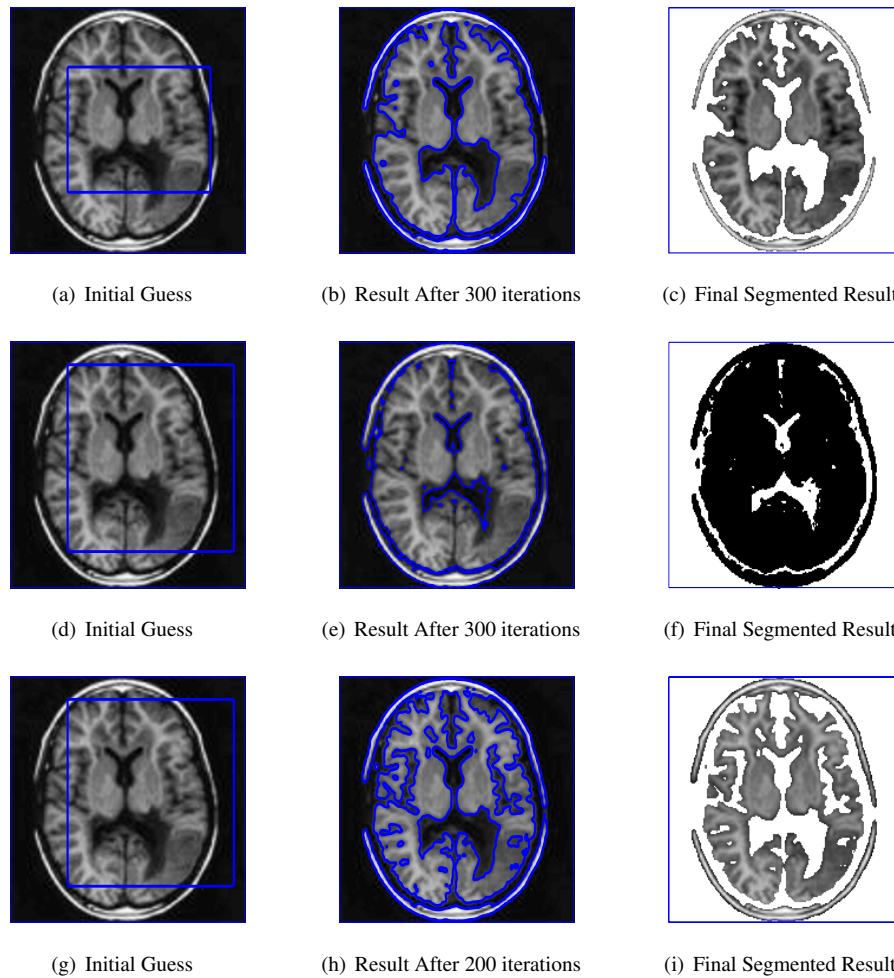


FIGURE 2. A real MR image of brain having inhomogeneity. Figure(c) and figure(f) shows the incomplete result of the CVB and MRS model respectively, while figure(i) represent the result of our proposed model. The parameters used for LSpf are:  $p = 6$  and  $\mu = 15$ .

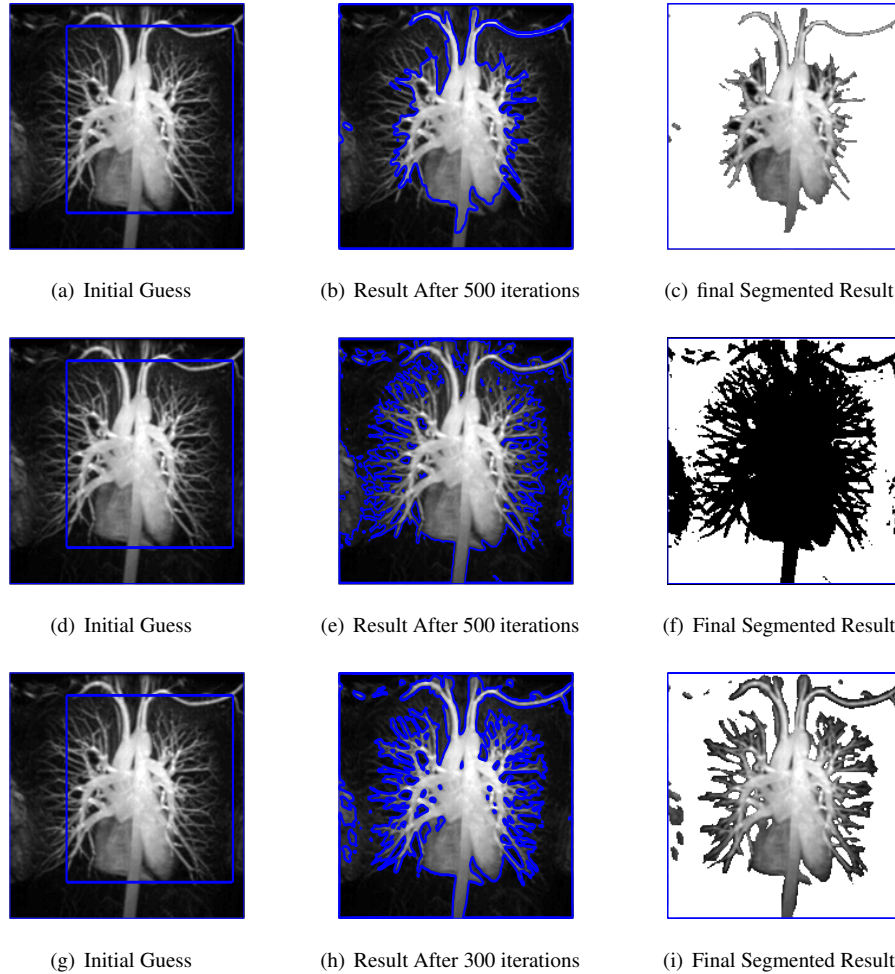


FIGURE 3. A heart image with inhomogeneous capillaries in which CVB and MRS fail to capture it as seen from figure(c) and figure(f) respectively, while LSpf capture the minute details. The parameters used for LSpf are:  $p = 4$  and  $\mu = 10$ .

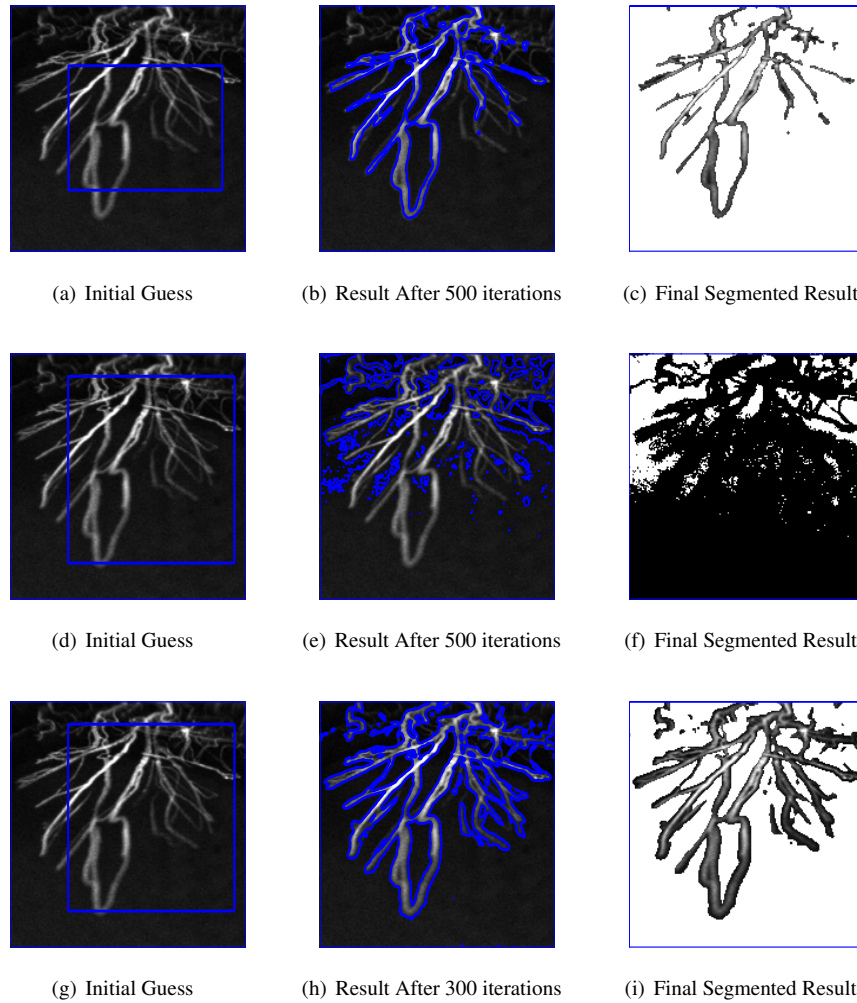


FIGURE 4. A inhomogeneous image of blood vessels in which CVB detect only prominent edges and MRS cannot work properly, while LSpf capture minute details as clear from figure(i). The parameters used for LSpf are:  $p = 2$  and  $\mu = 13$ .

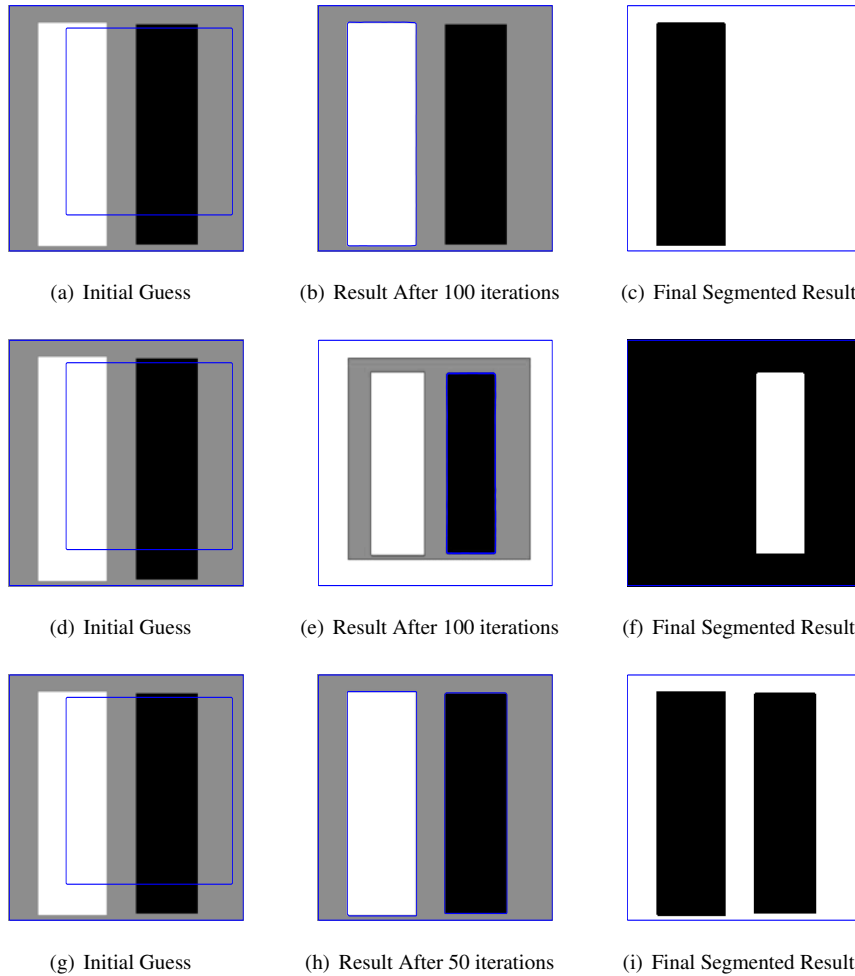


FIGURE 5. A synthetic image with average intensity background having two objects with maximum and minimum intensities in which CVB and MRS detect only one object, while LSpf capture both objects. The parameters used for LSpf are:  $\alpha = 150$  and  $\beta = 100$ .

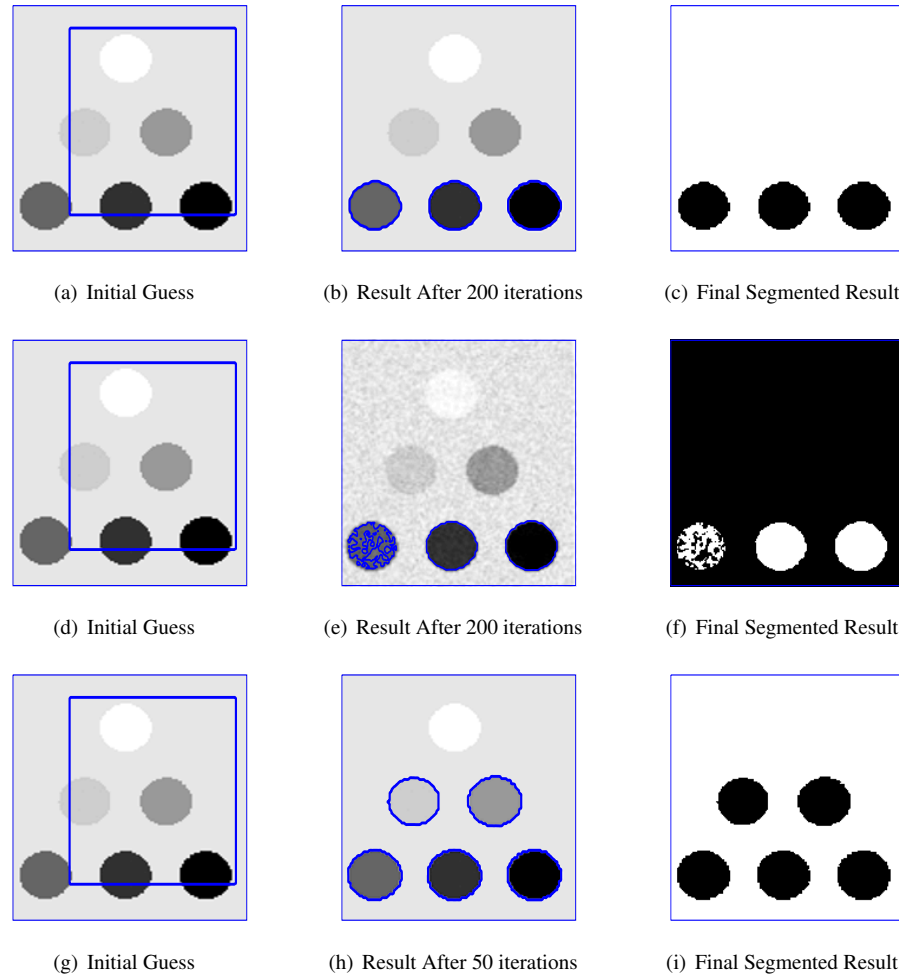


FIGURE 6. A synthetic image with average intensity background and having multi-intensities objects, in which CVB and MRS detect only three objects, while LSpf capture five of them. Although, the result of LSpf is also not satisfactory but better than CVB and MRS. The parameters used for LSpf are:  $\alpha = 130$  and  $\beta = 10$ .

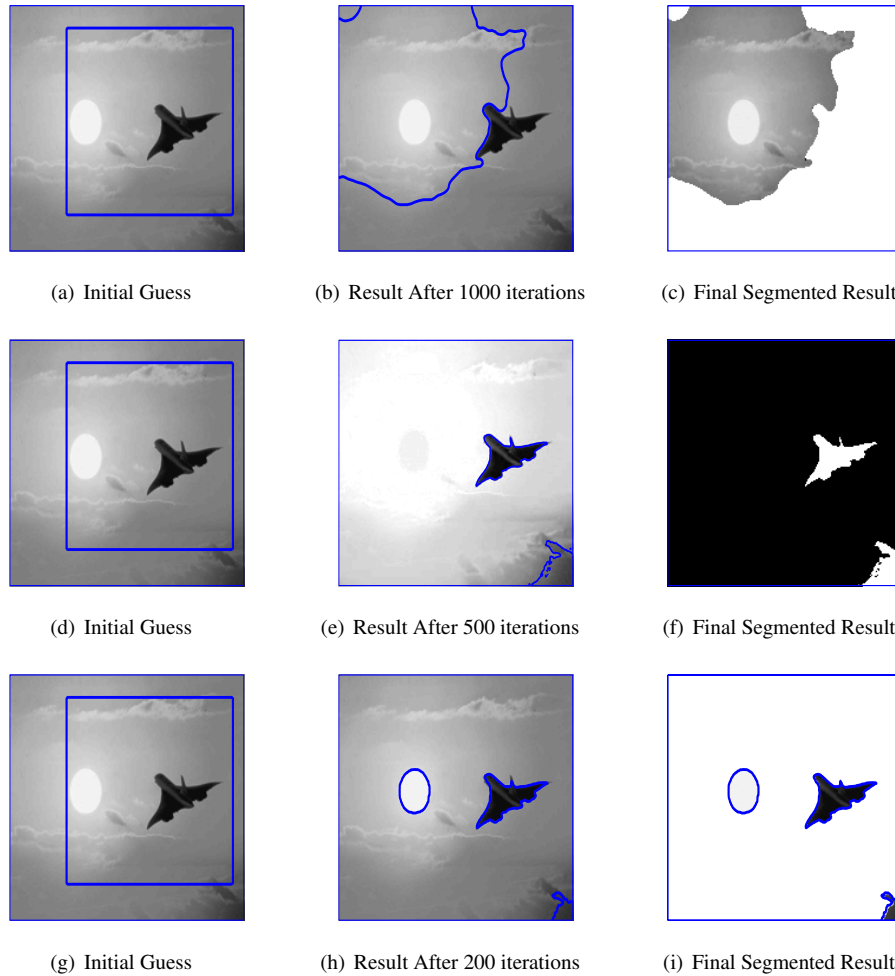


FIGURE 7. A real image of jet and sun having clouds in background, i.e. average intensity background. CVB completely fail to segment it as seen in figure(c) and MRS segment only one object as seen in figure(f), while LSpf segment it with also capturing an extra region as clear from figure(i), but LSpf result is much better than the others two. The parameters used for LSpf are:  $\alpha = 150$  and  $\beta = 150$ .

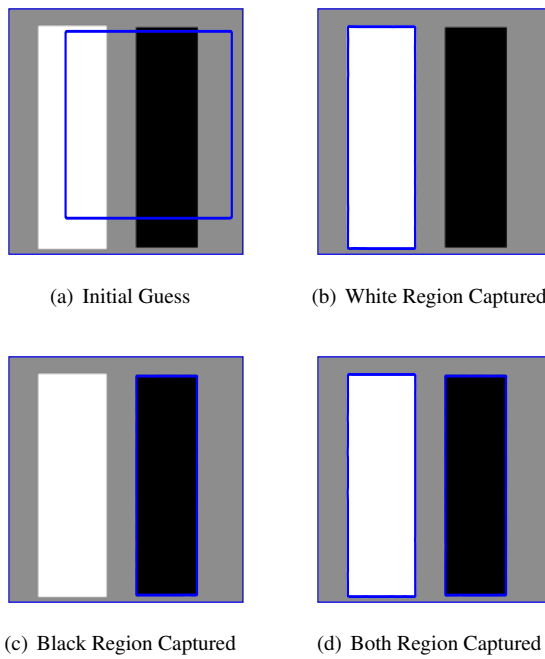


FIGURE 8. A synthetic image of multi-intensity objects having average intensity background is used to show the effects of parameters  $\alpha$  and  $\beta$ . The parameters used for (b)  $\alpha = 150, \beta = 50$ , (c)  $\alpha = 150, \beta = 150$  and (d)  $\alpha = 150, \beta = 100$ .